ST-former for short-term passenger flow prediction during COVID-19 in urban rail transit system

Shuxin Zhang, Jinlei Zhang, Lixing Yang, Chengcheng Wang, and Ziyou Gao

***Abstract*—Accurate passenger flow prediction of urban rail transit is essential for improving the performance of intelligent transportation systems, especially during the epidemic. How to dynamically model the complex spatiotemporal dependencies of passenger flow is the main issue in achieving accurate passenger flow prediction during the epidemic. To solve this issue, this paper proposes a brand-new transformer-based architecture called ST-former under the encoder-decoder framework specifically for COVID-19. Concretely, we develop a modified self-attention mechanism named Causal-Convolution ProbSparse Self-Attention (CPSA) to model the multiple temporal dependencies of passenger flow with low computational costs. To capture the complex and dynamic spatial dependencies, we introduce a novel Adaptive Multi-Graph Convolution Network (AMGCN) by leveraging multiple graphs in a self-adaptive manner. Additionally, the Multi-source Data Fusion block fuses the passenger flow data, COVID-19 confirmed case data, and the relevant social media data to study the impact of COVID-19 to passenger flow. Experiments on real-world passenger flow datasets demonstrate the superiority of ST-former over the other eleven state-of-the-art methods. Several ablation studies are carried out to verify the effectiveness and reliability of our model structure. Results can provide critical insights for the operation of URT systems.**

***Index Terms* — Deep learning, ST-former, Social media data, COVID-19, Short-term passenger flow prediction.**

I. INTRODUCTION

With the rapid expansion of the URT network and the increase in passenger flow, the spatiotemporal distribution of passenger flow has become complex increasingly. It is necessary to accurately and comprehensively analyze the passenger flow characteristics and take corresponding operation control measures in time, to ensure the safe and efficient operation of the URT system. Short-term passenger flow prediction can provide accurate and scientific data for the analysis of passenger flow characteristics, so it is significant to the operation and management of the URT system. On the one hand, accurate short-term passenger flow prediction can help passengers plan their travel reasonably and save travel costs. On the other hand, it can help operators adjust operation management strategies in real-time, and ensure safe and efficient operation of the URT system. Therefore, it is an important task to conduct accurate short-term passenger flow prediction.

Nowadays, an increasing number of studies have carried out short-term passenger flow prediction, and most of the existing studies focus on general daily passenger flow prediction. However, with the rapid spread of COVID-19 around the world, the passenger flows fluctuate more significantly than usual because of the complex and dynamic infectious features of the epidemic. Figure 1 shows the fluctuations in passenger flow during COVID-19. Specifically, in the early stage of COVID-19, passengers were generally reluctant to take the subway to reduce the risk of infection during travel, leading to a sharp drop in passenger flows in the URT system. With the COVID-19 epidemic under control, the passenger flow volume of URT has gradually increased. Therefore, it is a challenging task to conduct the accurate short-term passenger flow prediction during epidemic. Firstly, affected by the epidemic, the fluctuations of passenger flow are more random and complex, making the spatiotemporal dependencies of passenger flow hard to capture. Secondly, in the subway network, the passenger flow of a single station is not only influenced by itself but also interacts with that of other stations in the network. To achieve accurate passenger flow prediction, it is necessary to fully model the spatiotemporal relationships of passenger flow between each station of the network. Last but not least, external data sources, such as social media and the epidemic confirmed cases data, can reflect passengers' willingness to travel to some extent. How extract potential passenger flow evolution trends from these external data sources to improve the prediction accuracy is a key point to improve prediction accuracy.

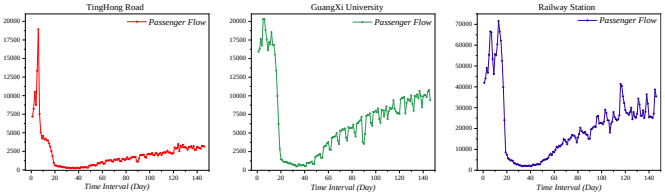

Figure 1 Variation of passenger flow in different stations during COVID-19

This work was supported by the National Natural Science Foundation of China (Nos. 72201029, 71825004), and the Shandong Provincial Department of Transportation Technology Project (No. 2021B68)

Shuxin Zhang, Jinlei Zhang, Lixing Yang, and Ziyou Gao are with the State Key Laboratory of Rail Traffic Control and Safety, Beijing Jiaotong University, No.3 Shangyuancun, Haidian District, Beijing 100044. (e-mail: 22110249@bjtu.edu.cn; zhangjinlei@bjtu.edu.cn; lxyang@bjtu.edu.cn; zygao@bjtu.edu.cn). Chengcheng Wang is with the engineer of Shandong Provincial Communications Planning and Design Institute Group Co. LTD, Jinan, 250101, China (e-mail: chengcheng.sdcpdi@foxmail.com).
(Corresponding author: Jinlei Zhang.)

To address these challenges, some scholars carried out relevant researches. For instance, Jiao and Huang (2021) considered the date attributes and the COVID-19 features, and then proposed an improved STL-LSTM model to predict the bus passenger flow during COVID-19. Lv and Li (2021) put forward a deep model to predict the urban traffic revitalization index, which integrated the data of the COVID-19 epidemic and traffic revitalization index of major cities in China. These researches achieved favorable prediction results and filled the gap in traffic prediction during COVID-19. However, the models of these researches were proposed for specific scenarios (bus passenger flow or urban traffic revitalization index). Due to the spatiotemporal dependencies of URT passenger flow are quite different from that of them, whether these modes are suitable for short-term URT passenger flow prediction during COVID-19 or not is to be explored. Hence, it is necessary to propose a specialized prediction method for the URT passenger flow during COVID-19.

In this study, we propose an architecture called ST-former based on the Encoder-Decoder framework for URT passenger flow prediction during COVID-19. In terms of the encoder, a novel Causal-Convolution ProbSparse Self-Attention (CPSA) is introduced to model the complex local temporal dependencies and changing features of historical inflow. A brand-new Adaptive Multi-Graph Convolutional Network (AMGCN) is developed to fully capture the multiple dynamic spatial dependencies of passenger flow, which applies multiple graph structures composed of the subway network stations. A Feature Extract Block is applied to reinforce the spatial-temporal features according to the results of CPSA and AMGCN and make a focused feature mapping in the next layer. In terms of the decoder, a Sequential Attention Block is introduced to integrate the temporal dependencies learned by the encoder and decoder. A Temporal Convolution Block is proposed to capture the dynamic long-term temporal dependencies and learn the dominant temporal features. In terms of the data sources, a Multi-source Data Fusion is proposed to fuse different external data sources. The social media data and the epidemic confirmed cases data are leveraged to study the impact of COVID-19 to passenger flow and reinforce the evolution features of passenger flow. For the historical passenger flow data, three patterns including weekly pattern, daily pattern, and real-time pattern are applied to capture the periodic features. Experiments on a subway network AFC dataset from a real city in China (after desensitization operation) show the superiority of ST-former. The main contributions of this paper are as follows.

1. The ST-former model is introduced to conduct the short-term URT passenger flow prediction during COVID-19. Under the Encoder-Decoder framework, several innovative blocks, including the Scalar Attention Embedding, CPSA, AMGCN, Feature Extract Block, and Temporal Convolution Block are proposed to capture the complex spatiotemporal dependencies of passenger flow simultaneously, thus improving the prediction accuracy.
2. We propose a Multi-source Data Fusion in the model architecture to fuse the epidemic confirmed case data and related social media data, which is beneficial to learn the impact of the epidemic to passenger flow and to reinforce the temporal features of passenger flow.
3. The ST-former model is tested on large-scale URT passenger flow datasets during COVID-19. Results show that our model outperforms the state-of-the-art methods in passenger flow prediction during COVID-19. Extensive ablation studies also show the effectiveness and robustness of our model framework.

The remainder of this paper is organized as follows. Section II reviews the related literature. The preliminaries are introduced in Section III. The methodology are described in Section IV. The experimental details and results are introduced in Section V, and the conclusions are summarized in Section VI.

II. LITERATURE REVIEW

In this section, the short-term passenger flow prediction methods, the traffic prediction using social media, and the Transformer applications are summarized.

2.1 Short-term Passenger Flow Prediction

Research studies on short-term passenger flow prediction have become increasingly prevailing in recent years, and the adopted methods range from conventional statistical methods to machine learning-based methods.

In the early stage, general statistical methods such as autoregressive integrated moving average model (ARIMA), exponential smoothing, and historical average (HA) were widely applied in traffic prediction tasks (Voort and Dougherty, 1996; Yang and Dillon, 2018). Specifically, Kumar and Vanajakshi (2015) proposed a seasonal ARIMA model for short-term traffic flow prediction under the conditions that the data was limited. Chen and Ye (2020) proposed an ARIMA-based model to predict the subway passenger flow for special events, which considered the dynamic volatility and nonlinearity of passenger flow during special events. Yang and Li (Yang and Li, 2021) made full use of ARIMA and optimization algorithm SA to fully capture passenger flow features, hence improving the prediction accuracy. These models have favorable prediction performance under some assumptions that the time series data is linear and stationary. However, most of the actual passenger flow does not conform to these assumptions, which limits the performance of these statistical models in practical applications.

With the rapid development of machine learning and data mining, such limitations were greatly overcome by machine learning-based models, such as support vector regression (SVR), k-nearest neighbor (KNN) model, and Kalman filter (Castro-Neto and Jeong et al., 2009; Guo and Huang, 2014). For example, Marco and Matteo (2013) developed two novel support vector regression models to capture typical traffic flow seasonality, thus achieving improvements in prediction accuracy and computational efficiency. Sun and Leng (2015) proposed Wavelet-SVM to decompose the passenger flow into high-frequency series and low-frequency series, and predicted them respectively, which improved the prediction accuracy. Cai and Wang (2016) utilized a spatiotemporal state matrix to

describe the traffic state and developed an improved KNN model to enhance traffic multistep forecasting accuracy. These machine learning-based models considered the temporal characteristics of traffic flow, thus improving the accuracy of prediction. Nevertheless, due to the weak ability to capture spatial information and long-term dependencies of traffic flow, they are inapplicable for large-scale network-wide prediction because the whole subway network contains highly dynamic and complex spatial topological information.

As a branch of machine learning, the emerging deep learning-based techniques have gradually become prominent methods in short-term passenger flow prediction. Since the long short-term memory network (LSTM) was firstly introduced in the traffic prediction field in 2015 (Ma and Tao et al.), an increasing number of deep learning-based models have been proposed for accurate traffic prediction. For instance, Ma and Dai (2017) regarded traffic speed data as images and proposed a classical convolutional neural network (CNN)-based method to predict large-scale, network-wide traffic speed. Zhang and Zheng (2017) developed an end-to-end structure, called ST-ResNet to collectively predict citywide crowd flows by modeling the temporal closeness, period, and trend properties of road traffic. Yao and Tang (2019) proposed a novel Spatial-Temporal Dynamic Network (STDN), which consists of a flow-gated local CNN and LSTM, to capture the spatial dependency and temporal periodicity. Considering that traffic networks are essentially graph-structures with topological characteristics, many scholars have integrated graph convolutional network (GCN) into prediction models to model the spatial dependencies. Specifically, STGCN (Yu and Yin, 2017) regarded the traffic network as a general graph to effectively model temporal dynamics and spatial dependencies of traffic flow. T-GCN (Zhao and Song et al., 2020) integrated the GCN and the gated recurrent unit (GRU) to capture the spatial and temporal dependencies simultaneously. Conv-GCN (Zhang and Chen, 2020) constructed a multi-graph GCN to deal with three inflow and outflow patterns (recent, daily, and weekly). However, the conventional GCN focuses on a predefined graph structure, which ignores the dynamic spatial dependencies among the nodes, resulting in a poor ability in modeling spatial correlation among the nodes. Therefore, some researchers have attempted to extend GCN for learning the dynamic hidden spatial dependencies. Res-RGNN (Chen and Li, 2019) utilized the graph-based spatial dependencies and temporal dynamics jointly to improve traffic prediction accuracy. Graph WaveNet (Wu and Pan, 2019) developed a novel adaptive dependency matrix through node embedding, which can overcome the limitation that fixed graph structure cannot reflect the dynamic spatial dependencies. Yu and Lee (2020) devised a novel graph-based neural network that expanded the general GCN to differentiate the connecting intensity of adjacent roads. Guo and Hu (2021) developed a graph-based network namely OGCRNN to construct an updating graph matrix for revealing the dynamic latent relationship of traffic flow. These modified GCNs effectively model the dynamic spatial dependencies to improve the prediction accuracy, which further indicates the importance of dynamic spatial dependencies for passenger flow prediction.

The prediction methods mentioned above have favorable prediction performance on general weekdays/weekends. However, due to the significant irregularity and suddenness of passenger flow during COVID-19, these methods may not effectively model the complex and dynamic spatiotemporal dependencies of the passenger flow, resulting in poor prediction performance. Thus, how to develop a prediction model taking the influence of COVID-19 into account seems to be the key to improving the URT passenger flow prediction accuracy during COVID-19.

2.2 Traffic Prediction Using Social Media

With the rapid development of social media, an increasing number of studies regarded social media data as an effective data source for the traffic prediction field, especially for predictions under special events (Chaniotakis and Antoniou, 2015). He and Shen (2013) proposed an optimization framework to extract traffic indicators based on tweet semantics and incorporate them into traffic prediction. This is the first time to integrate social media into traffic prediction. Ni et al. (2014) incorporated the tweet rate features and semantic features to predict the incoming traffic flow before sport game events. A few years later (2017), they further studied the correlation between social media and passenger flow and developed the optimization and prediction model with a hybrid loss function. This method combines social media and passenger flow under event occurrences to improve prediction accuracy. Chen and Lv (2019) introduced deep learning-based models to extract traffic information from social media, which can help detect traffic-related information. Yao and Qian (2021) mined Twitter messages to understand the impacts of people's work and rest patterns in the evening/midnight of the previous day to the next-day morning traffic. Roy and Hasan (2021) firstly considered the complex and dynamic nature of hurricane traffic evacuation, they then integrated Twitter data into prediction model for better capturing dynamic changes of traffic demand. Xue and Liu (2022) developed the multivariate disturbance-based hybrid deep neural network (MDB-HDNN) to model the disturbances of the subway passenger flow from social media post trends during events.

In summary, there are many methods applying social media to conduct traffic prediction under various events, which indicated that there is a great potential to leverage social media to explore the potential evolution trends of traffic flow. However, there is little research exploring how to apply social media to epidemic passenger flow prediction in URT. Hence, integrating the epidemic-related social media into prediction models might be an effective way to improve the prediction accuracy of subway passenger flow during COVID-19.

2.3 Traffic Prediction with Transformer

Transformer was originally proposed for natural language processing (NLP) in 2017 and achieved great success. In a parallel computing setting, Transformer makes advantage of multi-head attention mechanism to automatically capture the correlation of different representation subspaces in sequence data. Hence, Transformer-based methods are gradually applied in the field of time series prediction in recent years. For instance, Ye and Fang (2022) proposed a deep learning framework

named Meta Graph Transformer (MGT) to solve traffic prediction problems. This model takes the spatial-temporal heterogeneity into consideration, and makes full use of attention mechanisms in both temporal and spatial dimensions. Yan and Ma (2021) developed a novel traffic forecasting algorithm called traffic transformer, which consists of global encoder and global-local decoder to learn dynamic and hierarchical features in sequential data. To model the spatial and temporal correlations simultaneously, Zhang and Tsung (2021) developed a novel spatial-temporal synchronous self-attention layer. They also utilized multiple pre-defined graph structures to construct multi-view GCN for spatial dependence modeling. Zhou and Zhang (2020) designed an efficient transformer-based model, named Informer to address the long sequence time-series forecasting (LSTF) problem with high inference speed. This model overcomes several limitations with Transformer, such as quadratic time complexity and high memory usage, thus improving the prediction accuracy in LSTF.

The above literatures illustrate that there is a broad application prospect of transformer-based models in the traffic prediction field. These models can capture dynamic multiple temporal dependencies because of the multi-head attention mechanism, which is useful for time series processing. Therefore, it seems to be a feasible way to develop a transformer-based model for learning the temporal dynamics and randomness of passenger flow during COVID-19.

In this paper, we present a transformer-based approach combining passenger flow data and multi-source epidemic data to predict URT passenger flow during COVID-19.

III. PRELIMINARIES

We will introduce the preliminary knowledge in this section. The problem of short-term subway passenger flow prediction during COVID-19 will be first defined. Then we will briefly review the idea of ProbSparse attention mechanism and GCN as prerequisite knowledge to better understand our model.

3.1 Problem definition

The purpose of this study is to predict the short-term passenger flow of the URT system in the next time interval using historical information during COVID-19.

Definition 1 (Passenger Flow Matrix): Given an AFC record, which includes the passenger's card number, departure station, departure time, arrival station, and arrival time, the historical passenger flow series can be extracted and integrated into the passenger flow feature matrix at different time intervals, such as 10min, 15min, and 60min. Let $p_n(t)$ be the inflow data at the station *n* during the *t-th* time interval. The passenger flow feature matrix P^T can be defined as follows.

$$P^T = \begin{pmatrix} p_1(t-ts+1) & p_1(t-ts+2) & \cdots & p_1(t) \\ p_2(t-ts+1) & p_2(t-ts+2) & \cdots & p_2(t) \\ \vdots & \vdots & \vdots & \vdots \\ p_n(t-ts+1) & p_n(t-ts+2) & \cdots & p_n(t) \end{pmatrix} \quad (1)$$

where $P^T \in R^{N\times TS}$ denotes the observed inflow of the whole URT system at the *t-th* time interval, *N* denotes the number of the stations, and *TS* denotes the maximum time step at the *t-th* time interval. In this study, we select *12* as the maximum time step after fine-tuning.

Definition 2 (External Features matrix): Given the COVID-19-related social media data and the epidemic confirmed cases data, S^T and C^T can be defined as the observed data volume during the *t-th* time interval, such as the number of related social media and the number of confirmed cases. Notably, we hypothesize that the impact of social media and confirmed cases data remains the same for each URT station, and the observation period of the social media and confirmed cases data is consistent with that of passenger flow.

Definition 3 (Multiple Graphs): Based on specific domain knowledge (topology and similarity, etc.), multiple graphs can be constructed to express various spatial relationships between nodes (stations). In this paper, we take three spatial graphs into account, named adjacent graph, functional similarity graph, and origin-destination (OD) correlation graph of the URT network. These graphs are denoted as $G_a = (S, E_a, W_a)$, $G_s = (S, E_s, W_s)$, and $G_c = (S, E_c, W_c)$, respectively, where $S = \{s_1, s_2, \dots, s_n\}$ is the set of the stations, *n* is the number of the URT stations, and $e_{ij} \in E_k (k = a, s, c)$ are the edge between the station *i* and station *j* in G_k. To represent the multiple spatial dependencies of the whole URT network, we construct the multiple weight matrices W_k of $G_k (k = a, s, c)$.

1) Adjacent Graph*:* G_a is directly built according to the physical topology between the stations of the whole URT network. The edge $E_a(i,j)$ between station *i* and station j is constructed, if these two stations are connected in the real world. Meanwhile, if there exists $E_a(i,j)$ between station *i* and station j, $A(i,j) = 1$, or else $A(i,j) = 0$. The common definition of the adjacent-based weight between station *i* and station *j* is formulated as:

$$W_a(i,j) = \frac{A(i,j)}{\sum_{k=1}^{n} A(i,k)}, for\ i,j = 1,2,\dots,N \quad (2)$$

2) Functional Similarity Graph: In addition to the physical topology between stations, the functional similarity of the stations is also critical to model the spatial dependencies. Although some stations are far apart, they may be related to each other because of similar functions (such as commuter stations, and business stations). Thus, we take the functional similarity into account to further capture the spatial dependencies. Specifically, denote $\boldsymbol{x}_i^t \in R^{C\times TS}$ as the historical passenger features of the station s_i where *C* is the total number of passenger features and *TS* is the time step at the time interval *t*. In this paper, the total number of passenger features is 1, which is the passenger flow. The similarity weight between s_i and s_j can be defined as:

$$\widetilde{W_s}(i,j) = \frac{\sum_{t=1}^{T}(x_i^t - \overline{x_i})(x_j^t - \overline{x_j})}{\sqrt{\sum_{t=1}^{T}(x_i^t - \overline{x_i})^2}\sqrt{\sum_{t=1}^{T}(x_j^t - \overline{x_j})^2}} \quad (3)$$

Given similarity weight matrix $\widetilde{W_s}(i,j) \in R^{N\times N}$, we select some stations with high similarity weight to construct edges E_s.

We preset a similarity threshold $\hat{S}(i,j)$ to determine the stations as follows.

$$\widetilde{W_s}(i,j) = \begin{cases} \widetilde{W_s}(i,j), & if\ \widetilde{W_s}(i,j) > \hat{S}(i,j) \\ 0, & otherwise \end{cases} \quad (4)$$

Based on the corrected similarity weight matrix $\tilde{C}$, we adopt row-normalization to this matrix for easily training. The normalized matrix is calculated as follows.

$$W_S(i,j) = \frac{\widetilde{W}(i,j)}{\sum_{k=1}^{N} \widetilde{W}(i,k)}, for\ i,j = 1,2,\dots,N \quad (5)$$

3) OD Correlation Graph: Considering that the OD information of the target station can reflect the connection closeness between the target station and other stations, thus we extract the OD features between different stations from the raw AFC data to construct an OD correlation graph. Typically, the OD correlation coefficient from station s_i to s_j can be defined as follows.

$$\widetilde{W_c}(i,j) = \frac{count(i,j)}{\sum_{k=1}^{N} count(i,k)}, i,j = 1,\dots,N \quad (6)$$

where *count(i, j)* denotes the total number of passengers traveling from *i* to *j* and *N* is the total station number. Then we select some stations with high distribution ratio by comparing to a preset distribution ratio $\widetilde{W}_{OD}$.

$$\widetilde{W_c}(i,j) = \begin{cases} \widetilde{W_c}(i,j), & if\ \widetilde{W_c}(i,j) > \widetilde{W}_{OD} \\ 0, & otherwise \end{cases} \quad (7)$$

We also apply row-normalization to this matrix to build the OD correlation weight matrix as follows.

$$W_c(i,j) = \frac{\widetilde{W_c}(i,j)}{\sum_{k=1}^{N} \widetilde{W_c}(i,k)}, for\ i,j = 1,2,\dots,N \quad (8)$$

Thus, the passenger flow prediction in the whole subway network during COVID-19 can be formulated as follows.

Problem: Given the historical passenger flow matrix P^{T-1}, the social media feature vector S^{T-1}, the COVID-19 confirmed cases vector C^{T-1} and the URT network multiple graphs G_a, G_S, and G_c at the *(t-1)-th* time interval, the problem is to learn the mapping function *f* and predict the passenger flow y_t at the next time step *t*, as shown in equation:

$$Y_t = f(P^{T-1}, S^{T-1}, C^{T-1}, G_a, G_s, G_c) \quad (9)$$

where *f* indicates the model to be learned during training process.

3.2 ProbSparse Attention

In recent years, attention mechanisms have become increasingly prevailing in sequence data modeling (Child and Gray, 2019) , which allows to model the dependencies without regard to their distance in the sequence. Transformer (Vaswani and Shazeer et al., 2017) is one of the representative attention mechanism-based models. In this model, "Scaled Dot-Product Attention" was proposed to draw global dependencies between input and output. It can be regarded as a function mapping a query (Q) and a set of key (K)–value (V) pairs to an output. Specifically, given the queries and keys with dimension d_k, the values with dimension d_v, the Scaled Dot-Product Attention can be formulated as follows.

$$Attention\ (Q,K,V) = softmax(\frac{QK^T}{\sqrt{d_k}})V \quad (10)$$

where $Q \in R^{L_Q \times d_k}, K \in R^{L_K \times d_k}, V \in R^{L_V \times d_v}$ denotes the packed queries, values, and keys respectively.

However, recent studies (Child, 2019; Li and Jin et al., 2019) found that there exists potential sparsity for the distribution of attention weights between collection values. Some small attention weights between collection values may not significantly affect performance, but the calculation process will incur the computational cost and memory usage. In this case, the ProbSparse Attention is proposed to address these limitations by selecting only some dominant queries to interact with the keys. It can achieve favorable performance on sequences' dependencies calculation with low computational cost and memory usage. Specifically, to distinguish the "important" queries, the *i*-th query's sparsity measurement is defined as follows.

$$M(q_i,K) = ln \sum_{j=1}^{L_K} e^{\frac{q_i k_j^T}{\sqrt{d}}} - \frac{1}{L_K} \sum_{j=1}^{L_K} \frac{q_i k_j^T}{\sqrt{d}} \quad (11)$$

where the first term is the Log-Sum-Exp (LSE) of q_i on all the keys, and the second term is the arithmetic mean on them. L_K denotes the length of the *K*. If *i*-th query receives a larger $M(q_i,K)$, its "important" coefficient is much higher, and has a high chance to dominant in the sparse distribution. Based on the query's sparsity measurement, the ProbSparse Attention can only focus on *u* dominant queries:

$$ProbSparse\ Attention\ (Q,K,V) = softmax(\frac{\bar{Q}K^T}{\sqrt{d_k}})V \quad (12)$$

where $\bar{Q}$ denotes a sparse matrix with the same size of *Q* and it only contains the Top-*u* queries according to the sparsity measurement $M(q,K)$. The u is controlled by a constant sampling factor *c* under the formula $u = c \cdot lnL_Q$.

Performing a single attention function can only focus on information in a single representation space, whereas sequence data has different information in different representation subspaces. To jointly attend to information from different representation subspaces, the multi-head attention mechanism should be taken into consideration. Given the queries $Q \in R^{L_Q \times d_{model}}$, keys $K \in R^{L_K \times d_{model}}$, and values $V \in R^{L_V \times d_{model}}$, where d_{model} denotes the feature size of input, multi-head attention firstly linearly transforms the queries, keys, and values into different representation subspaces, then conducts the attention function in parallel. It can be formulated as follows.

$$MultiHead(Q,K,V) = Concat(Head_1, Head_2, \cdots, Head_H)W^o$$
$$Head_h = Attention(QW_h^Q, KW_h^K, VW_h^V) \quad (13)$$

where *H* is the number of attention heads, $W_h^Q \in R^{d_{model} \times d_k}, W_h^K \in R^{d_{model} \times d_k}, W_h^V \in R^{d_{model} \times d_v}$ are projection weight matrices applied to *Q*, *K*, *V*, and $W^o \in R^{H \cdot d_v \times d_{model}}$ is the final output projection matrix. In this paper, we set $d_k = d_v = d_{model} / H$.

3.3 GCN

The traffic network can be treated as a graph structure, where the stations can be treated as nodes and the links between stations can be treated as edges. Thus, it is reasonable to utilize

graph theory to deal with traffic networks. With the powerful ability to capture the spatial dependencies between the nodes of the graph, an increasing number of researchers applied GCNs to the traffic prediction field. The general idea of GCNs is to integrate the features of the adjacent nodes using their topological information to learn the target node representations. Firstly, GCNs aggregate the features of neighboring nodes to generate an intermediate representation. Then, this representation is dealt with by a linear projection with a non-linear activation function to derive the target node representation. We apply the GCN introduced by Kipf *et al.* (2016)in our model as follows.

$$Z^{l} = GCN\left(Z^{(l-1)}\right) = \sigma\left(\left(\widehat{D}^{-\frac{1}{2}}\tilde{A}\widehat{D}^{-\frac{1}{2}}\right)\cdot Z^{(l-1)}\cdot W^{(l-1)} + b^{(l-1)}\right) \quad (14)$$

where $Z^{(l-1)} \in R^{N\times d_{model}}$ denotes the input feature matrix of the $(l-1)^{th}$ layer, W^{l-1} denotes the weight matrix of the $(l-1)^{th}$ layer, $b^{(l-1)}$ denotes the bias of the $(l-1)^{th}$ layer, and $\sigma(\cdot)$ denotes the non-linear activation function. The $(\widehat{D}^{-\frac{1}{2}}\tilde{A}\widehat{D}^{-\frac{1}{2}})$ represents the calculation of normalized adjacency matrix, where $\tilde{A} \in R^{N\times N}$ denotes the adjacency matrix with self-loops, and $\widehat{D} \in R^{N\times N}$ denotes the diagonal degree matrix of $\tilde{A}$.

IV. MODEL STRUCTURE

4.1 Overview

The structure of the ST-former for short-term passenger flow prediction of URT system during COVID-19 is shown in Figure2. We apply an encoder-decoder architecture in the proposed model, and both the encoder and decoder consist of multiple identical sub-layers. In addition to the encoder-decoder structure, we develop Scaled Attention Embedding to convert the input to vectors with the intensive overall features before they are input into the encoder and decoder. Besides, we also propose Multi-source Data Fusion to capture the impact of social media and epidemic data on the evolution of passenger flow during COVID-19. The detailed components of ST-former are described as follows.

Within the encoder, each sub-layer consists of Causal-Convolution ProbSprase self-Attention (CPSA), Adaptive Multi-Graph Convolution Network (AMGCN), and Feature Extract block. Specifically, CPSAs are exploited to model the local temporal trend and the dynamic evolution of passenger flow with low computation and memory occupancy. AMGCN is utilized to model the dynamic spatial dependence according to multiple graphs in a self-adaptive manner. Feature extract block can reinforce the spatial-temporal features obtained from CPSA and AMGCN, and make a focused feature mapping in the next layer.

Within the decoder, each sub-layer consists of a Sequential Attention Block and Temporal Convolution Block. Specifically, sequential attention blocks are composed of masking CPSA and multi-head self-attention. Similar to the functionality of CPSA, masking CPSA is also applied to model the temporal dependencies of the decoder sequence while ensuring that each position of the left cannot attend to coming positions. The conventional self-attention is applied to allow every position in the decoder to attend to all positions in the input sequence temporally. Following the multi-head self-attention, a temporal convolution block is introduced to capture the dynamic long-term global temporal dependencies of the passenger flow. To enhance the trend features of passenger flow evolution during the epidemic and capture the impact of the epidemic on passenger flow, we propose Multi-source Data Fusion to fuse the processed passenger flow data, epidemic data, and related social media data.

Finally, the output of the decoder and the output the of Multi-source Data Fusion are fused into passenger flow feature data, and then the fully connected layer maps the passenger flow feature to the sample space to obtain the prediction value.

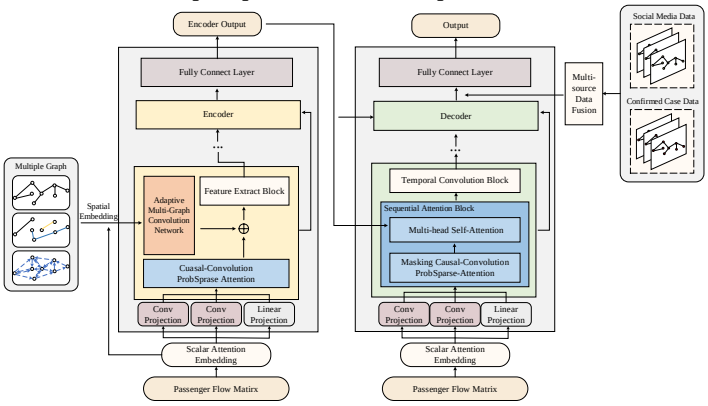

Figure. 1. The overview of the ST-former.

4.2 Scalar Attention Embedding

To refine the passenger flow features and facilitate sequence transduction, we develop a scalar attention embedding module to covert the passenger flow matrix $P^{T} \in R^{N\times TS\times 1}$ to the refine feature matrix $\widehat{P^{T}} \in R^{d_{model}\times N\times TS}$. Figure3 shows the overview of the scalar attention embedding. To our best knowledge that CNNs have significantly pushed the performance of feature tasks based on their rich representation power. Thus, it is feasible to utilize the convolution operation to improve the ability to represent features. Woo and Park (2018)proposed a convolutional block attention module (CBAM) to learn which features to emphasize or suppress, which can enhance the representation power of CNNs. Inspired by the favorable performance in feature representation of CBAM, we apply one of its components, named spatial attention module to refine the passenger flow feature representation. It should be noted that "spatial" here refers to the channel axis of the image, which is quite different from the "spatial" of the urban rail transit system.

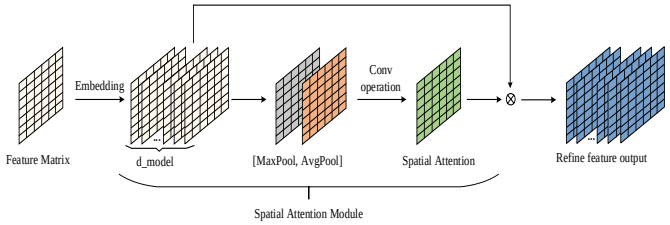

Figure 3 The overview of scalar attention embedding

The spatial attention module is developed to exploit the inter-spatial relationship of features. Since the passenger flow feature matrix is a 2D map, we first project the feature matrix into d_{model}-dim vector with 2D convolution filters to obtain the embedding matrix $\tilde{P}^T \in R^{d_{model} \times N \times TS}$. Applying the pooling operation along the channel axis (Woo and Park, 2018) has been proven to be effective in focusing on the important parts. Hence, we apply average-pooling and max-pooling operations along the channel axis for embedding matrix $\tilde{P}^T \in R^{d_{model} \times N \times TS}$ and then concatenate them to produce a feature map. After obtaining a feature map, we adopt a convolution layer to generate a spatial attention map $M_S(\tilde{P}^T) \in R^{1 \times N \times TS}$ which encodes the features to stress or suppress. The spatial attention can be computed as follows.

$$M_S(\tilde{P}^T) = \sigma(f^{7\times7}([AvgPool(\tilde{P}^T); [MaxPool(\tilde{P}^T)])) \quad (15)$$

where σ denotes the sigmoid activation function and $f^{7\times7}$ represents a convolution operation with the 7×7 filter. To refine the passenger flow features, we utilize the element-wise multiplication to project the spatial attention map $M_S(\tilde{P}^T)$ into the embedding matrix $\tilde{P}^T$, in which the broadcast mechanism is used to extend the dimension of the spatial attention map along the channel axis. The overall scalar attention embedding process can be summarized as:

$$\widehat{\tilde{P}^T} = M_S(\tilde{P}^T) \otimes \tilde{P}^T \quad (16)$$

where $\otimes$ denotes the element-wise multiplication, and $\widehat{\tilde{P}^T}$ is the refined feature matrix.

4.3 Encoder

The encoder stacks an input projection layer and multiple identical encoder layers. Each encoder layer consists of three components, namely Causal-Convolution ProbSparse Self-Attention mechanism (*CPSA*), Adaptive Multi-Graph Convolution Network (AMGCN), and Features Extract Block. To optimize the training process, the residual connection is adopted between each encoder layer. The causal-convolution probsparse self-attention (*CPSA*) is introduced to capture the local trend and the dynamic evolution of passenger flow. The novel adaptive multi-graph convolution network (AMGCN) is developed to explore the different types of hidden spatial dependencies in addition to the explicit spatial topology. The features extract block is proposed to focus on the features with high attention weight and make a concentrated feature mapping in the next layer.

4.3.1 Causal-Convolution ProbSparse Self-Attention

As we mentioned in section 3.2, multi-head probsparse attention enables to jointly attend to information from different representation subspaces. It provides an effective way to capture the complex temporal dependencies in multiple subspaces with low computation and memory occupancy, thus improving the ability of feature representation. However, the multi-head attention is originally proposed to process natural language, mainly for discrete data (e.g., words), resulting in its poor ability to capture the local trend features of continuous data (e.g., passenger flow data). Taking the passenger flow curve in Figure4 as an example, where A, B, and C represent the data points in different time periods, and the passenger flow of A and B are the same. In this case, if we utilize the initial multi-head attention to process the passenger flow, A and B will be given the higher correlation weight, since they have the same numerical value, while their local trends are significantly different. Although the numerical values of A and C are slightly different, they have similar local trend features, so there is a higher probability to have the same passenger flow pattern. Therefore, they should be given a higher correlation weight. It can be seen that utilizing the initial multi-head attention to process continuous time series data may lead to mismatches of correlation weight and unreasonable sequence representation.

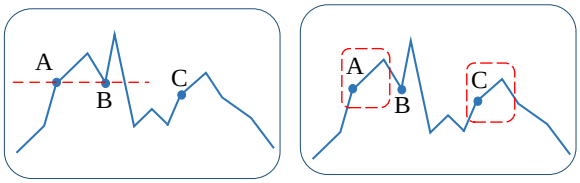

Figure 4 Local trend correlation

Inspired by the fact that convolution operations calculate the representations by conducting the local contextual context, we develop a multi-head causal-convolution probsparse self-attention (multi-head CPSA) to consider local evolution trend so as to address the mismatch problem caused by multi-head attention. Figure5 shows the calculation process of the multi-head CPSA. It is a variant of multi-head convolution self-attention (Zhang and Zhang, 2022), which replaces the linear projection of the queries and keys with 1D convolution operation before calculating the attention scores. In our case, we adopt the causal convolution instead of normal convolution to transform the queries and keys, avoiding the local evolutionary trend of the following position will be learned in advance. The causal convolution performs the convolution operation by only considering the historical information to the left of the current position, and it can also address the local temporal trend problem by a larger receptive field obtained from the "dilated" operation. Formally, our multi-head causal-convolution probsparse self-attention can be defined as follows.

$$MultiHead(Q,K,V) = Concat(ConvHead_1, ConvHead_2, \cdots, ConvHead_h)W^o$$
$$ConvHead_h = ProbSparse\ Attention(Q * \mathbb{C}_h^q, K * \mathbb{C}_h^k, V \cdot W_h^v) \quad (17)$$

where $\mathbb{C}_h^q$ and $\mathbb{C}_h^k$ denote the convolutional filter of Q and K, W_h^v denotes the projection weight matrix, " $*$ " denotes the causal convolution operation, " $\cdot$ " denotes the linear projection, and all the nodes share the weights.

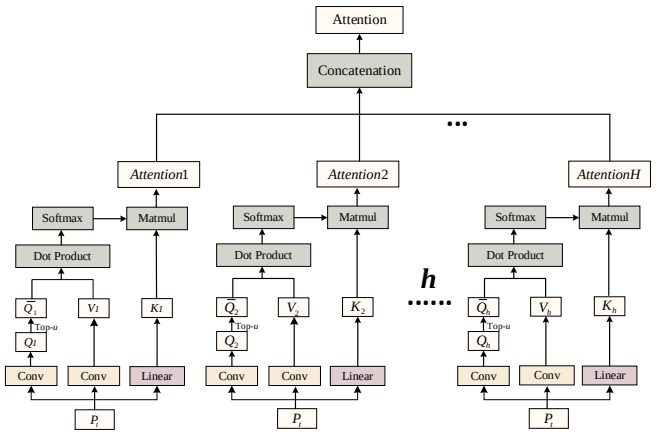

Figure 5 The visualization of CPSA

4.3.2 *Adaptive Multi-Graph Convolution Network*

The conventional GNNs mentioned above always rely on a single pre-defined adjacency matrix to construct the graph, and the weights assigned to the adjacent nodes are fixed during the learning process. However, the spatial dependencies between the nodes could change over time, and only relying on a single adjacency matrix cannot fully model the complex hidden spatial dependencies. For example, the nodes that are not connected physically may have the same passenger flow pattern, while the passenger flow of the adjacent nodes may not be associated. Thus, it might be not suitable to use such conventional GNNs to model the complex dynamic spatial dependencies of passenger flow.

Inspired by the work in Graph Transformer (Dwivedi and Bresson, 2020) and Graph WaveNet (Wu and Pan, 2019), we develop a novel adaptive multi-graph convolution network (AMGCN) based on a proposed self-adaptive adjacency matrix $\tilde{A}_{adp}$, and Figure6 shows the overview of AMGCN. Specifically, the self-adaptive adjacency matrix does not require any prior knowledge and is learned end-to-end through stochastic gradient descent. In our case, we firstly randomly initialize two node embeddings with learnable parameters $N_i, N_j \in R^{N\times d_{model}}$, then generate the self-adaptive adjacency matrix $\tilde{A}_{adp}$ as follows.

$$\tilde{A}_{adp} = Softmax(ReLU(N_i \cdot {N_j}^T)) \in R^{N\times N} \quad (18)$$

By multiplying N_i and N_j, the spatial dependency weights between node i and node j can be derived. The ReLU activation function can ignore the weak correlations, and the Softmax function is applied to normalize the self-adaptive adjacency matrix. In essence, the self-adaptive adjacency matrix is a supplement to the uncertain relations between the nodes. However, only using the self-adaptive adjacency matrix $\tilde{A}_{adp}$ not only cannot fully represent complex spatial dependencies, but also lacks of the model interpretability. Thus, adding extra prior knowledge might be a reasonable way to fully discover the hidden spatial dependencies and enhance the model interpretability.

In our case, we construct three types of graphs, namely adjacency graph $G_a = (S, E_a, W_a)$, functional similarity graph $G_s = (S, E_s, W_s)$, and OD correlation graph $G_c = (S, E_c, W_c)$, respectively, to represent the multiple spatial dependencies. These graph structures are firstly dealt with by a classical graph embedding technique named Eigenmaps (Mikhail and Partha, 2001) to transform the spatial embeddings $E_a^i, E_s^i, and\ E_c^i \in R^{N\times d_{model}}$ for node s_i. After calculating the spatial embeddings, a learnable approximate self-attention mechanism is performed to generate the spatial dependence weight matrices $S_a, S_s, and\ S_c$, and the ${S^{ij}}_b \in S_b (b = a, s, c)$ represents the corresponding spatial dependency between node i and node j.

$${S^{ij}}_b = softmax(\frac{E_b^i \cdot {E_b^j}^T}{\sqrt{d_{model}}}) \in R^{N\times N} \quad (19)$$

Given the self-adaptive adjacency matrix $\tilde{A}_{adp}$ and the spatial dependence weight matrices ${S^{ij}}_b \in S_b (b = a, s, c)$, we first conduct the graph convolution operation, and then transform the aggregated representation ${Z^l}_b\ (b = a, s, c)$ to the ultimate spatially informed output Z^l with a linear projection. The calculation process can be formulated as follows.

$${Z^l}_b = GCN({Z^{(l-1)}}_b) = \sigma\left((\tilde{A}_{adp} \oplus S_b) Z^{(l-1)} W^{(l-1)}\right)$$

$$Z^l = Linear(Concat({Z^l}_1, \cdots, {Z^l}_b)) \quad (20)$$

where $Z^{(l-1)} \in R^{d_{model}\times N\times TS}$ denotes the input feature matrix of the $(l-1)^{th}$ layer, $W^{(l-1)}$ denotes the weight matrix of the $(l-1)^{th}$ layer, $\sigma(\cdot)$ denotes the non-linear activation function, and $\oplus$ denotes the element-wise adding operation.

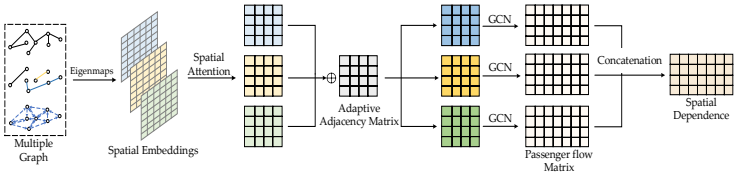

Figure 6 The overview of AMGCN

4.3.3 *Feature Extract Block*

Considering the sparsity of attention weights obtained by self-attention (only a few nodes have high attention weight, and others have little effect on the global sequence), the features extract blocks are proposed to emphasize the superior ones and make a focused feature mapping in the next layer, and Figure 7 shows the process of this block. Inspired by the Self-attention Distilling on Informer (Zhou and Zhang et al., 2020), our features "extraction" operation from the *j-th* layer into the *(j+1)-th* layer can be defined as follows.

$$X_{j+1}^t = MaxPool(ReLU\left(Attention\ Conv\ \left([X_j^t]_{SA}\right)\right)) \quad (21)$$

where $[\cdot]_{SA}$ represents the self-attention block, that is the causal-convolution probsparse multi-head self-attention, and $Attention\ Conv(\cdot)$ consists of channel attention module and the spatial attention module, which are the main components of CBAM mentioned above. The attention convolution operation can emphasize the meaningful features with high attention weights by integrating cross-channel and spatial attention. In $Attention\ Conv(\cdot)$, we sequentially adopt channel and spatial attention modules with the ReLU activation function, so that

each of branches can learn which information to highlight. Then we add a MaxPool layer to downsample X^t into its half slice after stacking a layer, which can focus on the dominant features and make the focused feature attention mapping in the next layer.

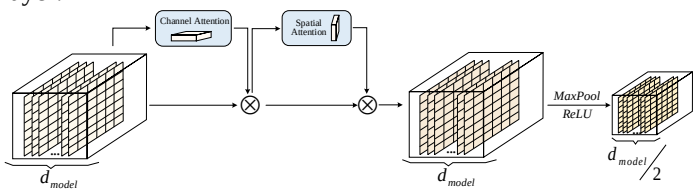

Figure 7 The process of Feature Extract Block

4.4 Decoder

The decoder stacks multiple identical decoder layers and an output projection layer. Each decoder layer consists of two components, namely Sequential Attention Block and Temporal Convolution block. In addition, the residual connection is utilized between the sub-layers to optimize the training process and accelerate model convergence.

4.4.1 Sequential Attention Block

Sequential Attention Block consists of Causal Convolution ProbSparse Self-Attention with Mask (Masking CPSA) and conventional self-attention blocks, which can integrate the spatial-temporal dependencies learned by Encoder and Decoder.

The CPSA with mask aims to capture the decoder sequence, and it works the same as CPSA. The only difference is that the masking operation is adopted to prevent each position from attending to coming positions. The mask is designed as a $T \times T$ matrix with elements above the diagonal taking the value $-\infty$ and others taking zero. Thus, the CPSA with mask can be modified as follows.

$$ProbSparse\ Attention\ (Q,K,V) = softmax(\frac{\bar{Q}K^T}{\sqrt{d_k}} + mask)V \quad (22)$$

The conventional self-attention block is introduced to connect the output of the encoder with each decoder layer. In this block, the queries come from the previous Masking CPSA, and the memory keys and values come from the output of encoder. It can allow every position in the decoder sequence to attend overall positions in the encoder sequence.

4.4.2 Temporal Convolution block

To capture the dynamic global temporal dependencies of the passenger flow and learn the dominant temporal features, we develop a Temporal Convolution block followed by the sequential attention block, which mainly consists of the dilated causal convolution (Lea and Flynn, 2017) and the temporal attention.

The conventional convolution operation realizes the learning of global temporal dependencies by stacking the convolution layer, resulting in a large computing cost. Thus, we conduct the "dilated" operation to expand the receptive field of the convolution process to calculate global historical information with a low computing cost. To avoid learning the temporal feature information ahead, we applied causal convolution in this block, which only considers the historical information to the left of the current position. Figure8 visualizes the dilated causal convolution operation.

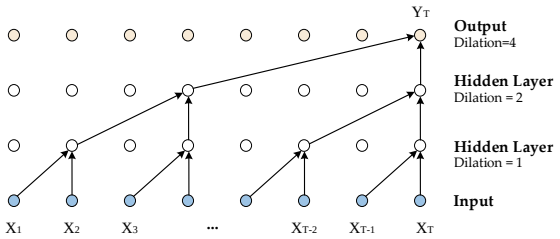

Figure 8 Visualization of the dilated causal convolution network

In addition to dilated causal convolution, we also apply the temporal attention to extract the meaningful temporal features (such as the peak values and edge values) along the temporal dimension. The *MaxPool* and *AvgPool* operations are conducted to obtain the temporal attention weights along the temporal axis, then the element-wise multiplication is utilized to capture the significant temporal features according to the temporal attention weights.

4.5 Multi-source Data Fusion

Multi-source data fusion aims to fuse the epidemic data and social media data with historical passenger flow to reinforce the trend features of passenger flow evolution over time and describe the impact of the epidemic to passenger flow. Figure10 shows the overview of the multi-source data fusion block. The ST-former without multi-source data fusion leads to poor performance in our experiment (see Section 5.4.4 for details), which indicates that the multi-source data fusion is indispensable to our model.

Before we introduce the multi-source data fusion block, we first study whether there is a potential relationship between the passenger flow data, the confirmed cases data, and the social media volume during COVID-19 (shown in Figure 9). We calculate their correlation coefficients of them through *SPSS*. The results of the correlation are shown in Table I, in which all the absolute values of Pearson coefficients are above 0.55 and significant. Specifically, the Pearson coefficient between the passenger flow and social media volume during COVID-19 is -0.814, indicating that there exists a significant negative correlation between them. The Pearson coefficient between the passenger flow and the confirmed cases data during COVID-19 is -0.585, which indicates there also exists a moderate negative correlation between them. Thus, we reasonably believe that these additional data sources can help improve the performance of the short-term URT passenger flow prediction during COVID-19.

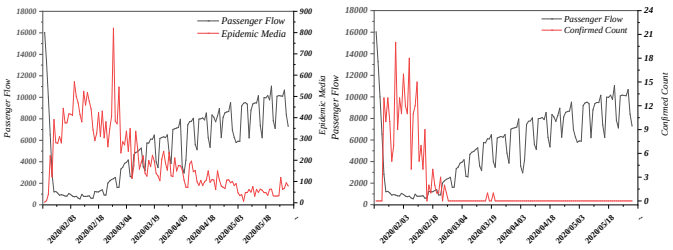

Figure 9 The comparison of passenger flow, epidemic confirmed cases data, and related social media

Table I Correlation of passenger flow, the number of confirmed cases, and social media volume

Data type	Pearson coefficient
Confirmed cases	-.585**
Epidemic social media	-.814**

Notes: **: p < 0.01.

In our multi-source data fusion block, we proportionally allocate the correlation weights of social media data and epidemic data in the modeling process according to the correlation analysis for fusing these data reasonably. Specifically, the social media data and the epidemic confirmed data are mapped into a 4-dimensional feature matrix, and then the channel dimension is linearized into 5 channels, in which the proportion between social media data and epidemic confirmed data is 3:2. After the proportional allocation process, the feature matrix is dealt with by the 2D convolution with the 3×3 kernel, aiming to capture the temporal features and make the dimension of auxiliary feature matrix consistent with that of the passenger flow matrix. Furthermore, we apply the pooling operation along the temporal dimension of the auxiliary feature matrix to refine the temporal trend features of passenger flow, and the auxiliary feature matrix is finally concatenated to the passenger matrix to complete the process of multi-source data fusion.

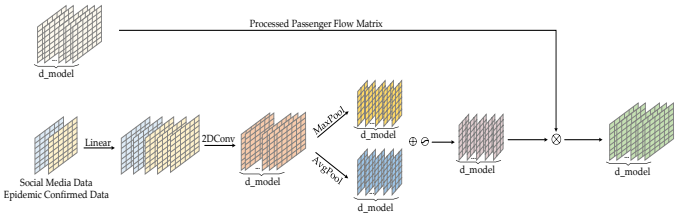

Figure 10 The overview of Multi-source Data Fusion

4.6 Multiple Periodicities

Since passenger flows usually have an obvious periodicity, we thus further consider two types of periodic patterns hidden in the historical passenger flow, namely weekly periodicity, and daily periodicity. The weekly periodicity refers to the similar characteristics of passenger flow at the same time period of each week, which is mainly caused by the regularity of human activities, such as commuting and schooling. The daily periodicity refers to the continuity of passenger flow characteristics of the adjacent two days. For instance, the passenger flow on the adjacent two weekdays has similar peak trends. To accurately describe the periodic characteristics of passenger flow, we introduce another two data types in addition to the regular historical passenger flow in the past *TS* time steps.

Weekly periodicity: To capture the weekly periodicity, we consider the *TS* time steps of passenger flow from the same time period in the last week as the present day, and it can be represented as $P_w^T \in \mathbb{R}^{N \times TS}$. In our paper, the time period we study is from 6:00 to 23:0, totally 17 hours, we suppose the time lag is *tl*, the time step is *ts*, and the current time slice is *t*, thus the weekly periodic can be formulated as:

$$P_w^T = (p_N\left(t - \left(\frac{17*60}{tl} * 7\right) - ts + 1\right), p_N\left(t - \left(\frac{17*60}{tl} * 7\right) - ts + 2\right), \cdots, p_N\left(t - \left(\frac{17*60}{tl} * 7\right) - 1\right)) \quad (23)$$

Daily periodicity: Analogously, to capture the daily periodicity, we also take the *TS* time steps of passenger flow from the same time period in the yesterday into consideration to obtain the daily periodic tensor $P_d^T \in \mathbb{R}^{N \times TS}$. It can be formulated as:

$$P_d^T = (p_N\left(t - \left(\frac{17*60}{tl}\right) - ts + 1\right), p_N\left(t - \left(\frac{17*60}{tl}\right) - ts + 2\right), \cdots, p_N\left(t - \left(\frac{17*60}{tl}\right) - 1\right)) \quad (24)$$

Once we obtain the weekly periodic tensor P_w^T and the daily periodic tensor P_d^T, we concatenate them with the past *TS* time steps tensor P_c^T, resulting in a new passenger flow feature tensor $P^T \in R^{N \times (3*TS)}$ as the input of our model. Figure11 shows these three types of passenger periodic feature tensors along the time axis.

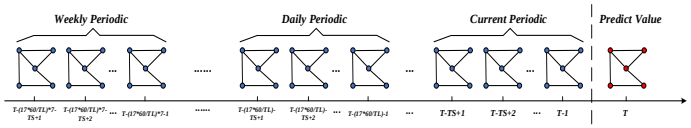

Figure 11 Three types of passenger periodic feature tensor

5 EXPERIMENTS

In this section, the ST-former framework and other eleven benchmark methods are tested on real-world urban rail transit AFC datasets in a Chinese city (CityMetro) under different time intervals. We first introduce the detail of CityMetro datasets, the model configurations and evaluation metrics, and the benchmark methods, then we illustrate the experiment results. In addition, the impact of the key components of ST-former on the prediction performance are also analyzed.

5.1 Dataset

To validate our proposed model, comprehensive experiments are carried out on real-world larger-scale urban rail transit AFC datasets, named CityMetro. Table II provides a summary of the statistical data. In our paper, we chose the AFC data from January 6 to May 31 (roughly five months) to match the COVID-19 development timeline, which covered the outbreak, stabilization, and improvement of the epidemic. Our experiments focus on the data from 6:00 to 23:00 with a total of

61 stations, and the inbound flow are aggregated by different time intervals of 10, 15, 20, 30, and 60min, resulting in a total of 102, 68, 51, 34, and 17 intervals in a day, respectively.

We also crawl the social media data (including text, time, geographical labels, etc.) with the keywords "COVID-19" and the city name from Sina microblog (a social platform) in a specific period, which was consistent with the period of passenger flow. Besides, we collect the corresponding epidemic confirmed cases data from the National Health Commission of the People's Republic of China. The time period of epidemic data is the same as that of passenger flow data.

Table II Dataset Description

Dataset	CityMetro				
Date	January 6, 2020, to May 31, 2020				
Time in a day	6:00-23:00				
Station Num	61				
Time interval	10min	15min	20min	30min	60min
Week number	21	21	21	21	21
Day number	147	147	147	147	147
Time slice in a day	102	68	51	34	17
Total time slice	14994	9996	7497	4998	2499

5.2 Model configurations and evaluation metrics

Model Configuration: In this experiment, we split the dataset at a ratio of 12: 4: 5 into training sets, validation sets, and test sets by the time. All data are normalized into the range [0, 1] with Min-Max normalization scalers and fed the normalized data into ST-former. We use the PyTorch framework to implement ST-former, which stacks up with three encoder layers and three decoder layers. For better training, dropout layers with a probability of 0.1 are added to encoder and decoder, respectively. The optimizer is Adam with a learning rate of 0.0001.

We also investigate the other four hyperparameters of ST-former in detail, such as the feature size of the model d_{model}, the number of heads *H*, the number of previous time steps *TS*, and the batch size. For optimal prediction performance, we set a section for the feature size of the model d_{model} as (24, 48, 64, 72). The number of heads *H* of the multi-head attention mechanisms no matter in the encoder or decoder are consistent, which is set as indicated in (3, 4, 6, 8). We also set a section for the number of previous time steps *TS*, ranging from 10 to 15. The batch size is set as (32, 48, 64, 128). In the hyperparameter tuning process, we follow the control variable principle, which means that only one hyperparameter will be tuned while the remaining hyperparameters remain constant until we find the best result. In this case, we take 60 minutes as a time step, and the results are shown in Figure12. According to the results, we can see that when the feature of the model d_{model}, the number of heads *H*, the number of previous time steps *TS*, and the batch size are set as 24, 3, 12, 32, respectively, SF-former achieves the best prediction performance.

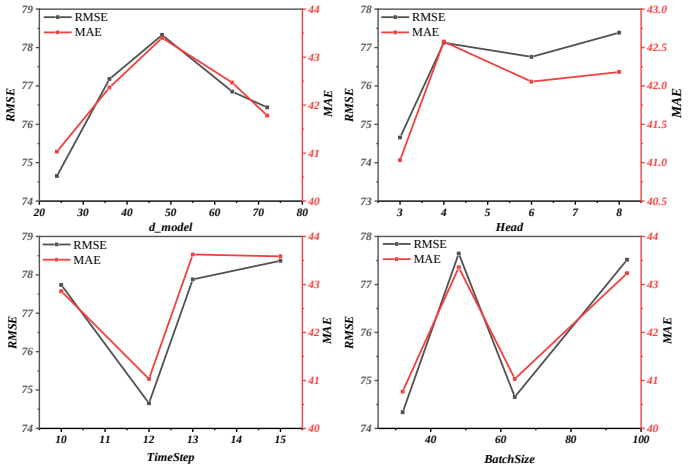

Figure 12 Hyperparameters tunning results

Evaluation Metrics: We chose the mean square error (MSE) as the loss function. To evaluate the prediction performance, we use the root mean square error (RMSE), mean absolute error (MAE), and weighted mean absolute percentage error (WMAPE) as evaluation metrics. The definitions of them are as follows.

$$loss = MSE = \frac{1}{m}\sum_{i=1}^{m}(y_i - \hat{y}_i)^2 \tag{25}$$

$$RMSE = \sqrt{\frac{1}{m}\sum_{i=1}^{m}(y_i - \hat{y}_i)^2} \tag{26}$$

$$MAE = \frac{1}{m}\sum_{i=1}^{m}|(y_i - \hat{y}_i)| \tag{27}$$

$$WMAPE = \sum_{i=1}^{m}\left\{\frac{y_i}{\sum_{j=1}^{m} y_i}\left|\frac{y_i - \hat{y}_i}{y_i}\right|\right\} \tag{28}$$

where $\hat{y}_i$ is the predicted values and y_i is the actual values, and *m* denotes the total number of all real values. The lower the evaluation metrics are, the better the prediction performance of the model is.

5.3 Benchmark Model

To comprehensively evaluate the prediction performance of our proposed model, eleven benchmark models are considered in our experiments, and the details of these models are described as follows.

- **Autoregressive Integrated Moving Average (ARIMA):** As a typical statistical model, ARIMA has been widely applied in time series processing. The three parameters of ARIMA, namely lag order, the degree of difference, and the order of the moving averages, are set to 2, 1, and 1, respectively after fine-tuning.
- **Long Short-Term Memory Neural Network (LSTM):** As a variant of RNN, LSTM was first applied in traffic prediction in 2015 (Ma and Tao et al.). We develop an LSTM-based model with two hidden layers and one fully connected layer. Each LSTM hidden layer has 64 neurons, and the fully connected layer has 61 neurons. The optimizer is Adam with a learning rate of 0.0001. We utilize the passenger flow during COVID-19 to train the model. The inputs are the inflow series of a total of 61 stations in the last

12-time step. The outputs are the inflow series of 61 stations at the next time step.

- **2D Convolution Neural Network (2DCNN):** We apply a general 2D CNN model with one CNN layer and one fully connected layer. The CNN layer has 8 filters. The kernel size is 3*3, the padding is 1, and the stride is 1, respectively. The fully connected layer has 61 neurons. The other settings are the same as that of LSTM.
- **Temporal Graph Convolutional Network (T-GCN):** This model is proposed by Zhao (2020), which combined the GCN and GRU to obtain the spatiotemporal correlation. We develop a T-GCN model with three hidden layers and one fully connected layer. The fully connected layer has 61 neurons. The parameters of T-GCN sub-layers are the same as that of the original model. The other settings are the same as that of LSTM.
- **Spatio-Temporal Residual Networks (ST-ResNet):** This model adopted the residual convolution units to model the temporal closeness. We only adopt three branches of residual networks and did not use external factors (weather, date attributes, etc.). The parameters of the model are consistent with Zhang's (2017).
- **ConvLSTM:** Proposed by Shi (2015), ConvLSTM achieved success in the prediction field. We construct a ConvLSTM model with three hidden layers and two fully connected layers. The first fully connected layer has 128 neurons and the second fully connected layer has 61 neurons. The other settings are the same as that of LSTM.
- **Diffusion Convolutional Recurrent Neural Network (DCRNN):** This framework is proposed (Li and Yu, 2017)to model the traffic flow as a diffusion process on a directed graph for learning the spatial dependency, by using bidirectional random walks. They also utilized the encoder-decoder architecture with scheduled sampling to capture temporal dependency. We implement DCRNN based on its public code. The other settings are the same as that of LSTM.
- **Graph WaveNet (GWN):** GWN (Wu and Pan, 2019) developed an adaptive dependency matrix to capture dynamic spatial correlation and utilized a stacked dilated 1D CNN to learn temporal features. We implement GWN based on its public code. The other settings are the same as that of LSTM.
- **Transformer:** This model was originally proposed (Vaswani and Shazeer et al., 2017) for natural language processing (NLP), and it was gradually applied in time series processing. We apply the conventional Transformer framework with a total of three layers. In each layer, we adopt eight multi-head attention, the values of d_k and d_v are all set to 64. The output of the Transformer is put into two fully connected layers. The first fully connected layer has 128 neurons and the second fully connected layer has 61 neurons. The other settings are the same as that of LSTM.
- **Meta Graph Transformer (MGT):** This model is a generalization of the original Transformer (Ye and Fang, 2022), which includes three types of attention layers named Temporal Self-Attention, Spatial Self-Attention, and Temporal Encoder-Decoder Attention, respectively. We implement MGT based on its public code. The other settings are the same as that of LSTM.
- **Informer:** Based on the Transformer, Informer (Zhou and Zhang et al., 2020) has been proven to be better at processing long sequence time-series forecasting. We utilize the Informer framework, where the encoder and decoder have three layers respectively. In each layer, we have eight heads to calculate multi-head attention, and the values of d_k and d_v are all set to 64. The other settings are the same as that of LSTM.

5.4 Experiment results and analysis

5.4.1 Overall analysis

The prediction performance of different methods on CityMetro is shown in Table III and Figure 13. According to the Table III, ST-former outperforms the benchmark methods in all cases. At the 10-minute time granularity, ST-former improves the state-of-the-art methods by 3.95%, 2.95%, and 3.04% in terms of MAE, RMSE, and WMAPE, respectively. Similar improvements can also be seen at the 15-minute time granularity, 20-time granularity, 30-time granularity, and 60-minute time granularity. We also can conclude that as the time granularity increasing, the prediction performance advantage of ST-former also increases gradually.

Specifically, the mathematical statistics-based model ARIMA performs the worst in every scenario, because it can only handle stationary time series and capture limited correlations. Due to the complicated function forms and effective feature-extracting abilities of deep learning-based models, they typically outperform the statistics-based model ARIMA in Table III. However, the effectiveness of a deep learning-based model is generally influenced by its structure. For example, the standard CNN and LSTM-based models perform the worst among the deep learning-based models mentioned in the Table, because CNN generally models the spatial features by convolution operation but ignores some temporal features, while LSTM generally models the temporal features through recursion operation but ignores some spatial features.

Compared with single-structure deep learning models, composite deep learning-based models are often more competitive in feature modeling. For example, T-GCN, a typical GCN-based method, employs GCN and GRU to capture spatiotemporal correlations, which outperforms CNN and LSTM in the experiment. However, limited by the ability of GCN to capture the dynamic spatial dependencies, its prediction accuracy is much lower than our method ST-former. DCRNN takes advantage of RNN to capture temporal

correlations and utilizes graph convolution with bidirectional random walks for spatial dependencies extraction, while one predefined adjacent matrix seems insufficient in capturing dynamic spatial correlations of a traffic network. ConvLSTM integrates the convolution structure into LSTM to capture the temporal correlations and spatial dependencies simultaneously, while lacking of modeling the graph structure limits the model's ability to capture complex spatial dependencies. ST-ResNet employs convolution-based residual networks to model the spatial dependencies and applies three residual networks to model the temporal closeness, period, and trend properties. Similarly, it also does not consider the graph structure, leading to poor ability to capture dynamic spatial dependencies. Graph WaveNet develops a self-adaptive graph convolution to address the problem caused by GCN, and utilizes TCN to capture the long-term temporal dependencies. However, lacking of any prior knowledge makes the model less interpretable.

The transformer-based methods utilize the multi-head self-attention to model the multiple temporal dependencies. However, as the memory bottleneck in stacking layers for long inputs of Transformer, it is not suitable for long-term series sequence processing. Informer improves the weaknesses of Transformer by developing a novel probsparse attention mechanism, and maintains the high prediction ability with lower computation and memory usage. However, both two models ignore the spatial dependencies of passenger flows, resulting in unfavorable prediction performance in several cases. Another transformer-based model MGT integrates the multiple graphs into the model, and considers the spatial and temporal heterogeneity simultaneously. However, this model suffers from the same problem as Transformer, where the long inputs lead to memory bottlenecks. Thus, MGT does not achieve favorable prediction performance.

Compared with the above methods, ST-former achieves the best performances in the five different time granularities. In this model, we develop Causal-Convolution Probsparse Self-Attention (CPSA) to model the complex temporal dependencies. Not only the current temporal periodic but also the daily and weekly periodic are fused into ST-former to fully capture the global periodicity of passenger flows. In addition, we make full use of the domain knowledge to develop a novel Adaptive Multi-Graph Convolution Network (AMGCN) to consider the dynamic spatial dependencies with multiple hidden patterns (physical connectivity, functional similarity, OD-based correlation). Besides, we introduce a Feature Extract Block to strengthen the representation of spatiotemporal features obtained by CPSA and AMGCN. Further, we fuse the passenger flow data, the epidemic confirmed data, and the related social data to study the impact of COVID-19 on passenger flows and reinforce the changing characteristics of passenger flow over time by the multi-source data fusion. Experimental results verify the superiority of our model.

5.4.2 Comparison of a single station

Since different subway stations have different passenger flow patterns, the prediction performance of passenger flows in different stations is distinguished. In this paper, we select three different types of stations to verify the station-level prediction performance of ST-former, and the results for different stations are reported in Figure14 (taking the prediction performance of passenger flow in one week as an example). Due to the desensitization of the CityMetro dataset, we refer to the following three stations as Station A, Station B, and Station C. Station A is adjacent to the main business district. Station B is a typical commuter station with many passengers living nearby. Station C is a large transfer hub that can achieve transfer among various modes of transportation.

Although these three stations have different passenger flow patterns, they have all seen a decline in passenger flow during COVID-19. Specifically, the prediction result of Station A that is the main business district is shown in Figure13 (a), and it can be seen that ST-former has a favorable prediction performance. During weekdays, the passenger flows present obvious morning and evening peak characteristics, and the passenger flow in the evening peak is significantly higher than that in the morning peak. During weekends, people do not have to go to work, so the passenger flow on weekends is not as much as that on weekdays. However, since the station is adjacent to the main business center, people will come here to relax on the weekends. Therefore, the passenger flow increases from the afternoon to the evening on weekends. In our model, CPSA can fully capture the local temporal trend features of passenger flow, especially for the local peak prediction. The temporal convolution block fits the overall trend of passenger flow by utilizing the convolution operation, which can improve the feature representation. Thus, ST-former achieves great prediction performance from both local and global perspectives.

Figure13 (b) reports the passenger flow prediction result of Station B, which is a typical commuter station. It can be seen that our model shows favorable performance no matter for the overall trend prediction or local fluctuation characterization of passenger flows. During weekdays, this station presents obvious characteristics of morning and evening peaks, while different from Station A mentioned above, the passenger flow at the morning peak is significantly higher than that of the evening peak. During weekends, the passenger flow on Saturdays still has commuting characteristics because of overtime. People usually rest on Sunday, so the passenger flow on Sunday has no obvious commuting characteristics. The feature extract block in ST-former can effectively study the periodic characteristics of passenger flow in the commuter station and emphasize meaningful features (local peak value and edge value). Therefore, ST-former has achieved favorable performance in the passenger flow prediction of Station B.

Table III Performance comparison of different methods on dataset CityMetro. The best results are emphasized in bold font and the second-best results are labeled with "+".

Time	Metric	ARIMA	LSTM	CNN	T-GCN	DCRNN	ConvLSTM	GWN	ST-ResNet	Transformer	MGT	Informer	ST-former
10min	RMSE	31.355	19.051	19.323	18.609	18.769	18.246	18.074	18.095	17.757+	19.601	18.142	**17.543**
	MAE	16.325	10.376	10.597	10.225	10.309	9.962	10.013	9.920	9.789+	10.701	10.172	**9.614**
	WMAPE	28.47%	17.89%	18.24%	17.63%	17.78%	17.15%	17.27%	17.10%+	16.83%+	18.41%	17.52%	**16.58%**
15min	RMSE	46.279	26.959	25.391	25.381	26.589	24.902	26.44	24.725+	25.777	28.627	24.738	**23.910**
	MAE	23.881	14.980	13.885	14.029	14.279	13.534	14.158	14.009	14.283	15.351	13.520+	**13.066**
	WMAPE	27.92%	17.34%	16.08%	16.22%	16.45%	15.56%	16.30%	16.08%	16.30%	17.62%	15.46%+	**14.95%**
20min	RMSE	62.575	33.461	33.465	32.304	35.354	33.051	35.731	32.033	35.271	40.619	31.872+	**30.265**
	MAE	32.903	17.940	17.998	17.758	19.361	17.977	19.403	17.234+	19.553	22.811	18.370	**16.707**
	WMAPE	28.05%	15.47%	15.47%	15.27%	16.68%	15.50%	16.77%	14.82%+	16.85%	19.77%	15.80%	**14.36%**
30min	RMSE	108.052	45.269+	45.474	48.047	55.141	49.534	52.259	46.856	67.961	57.983	45.752	**42.040**
	MAE	56.888	24.876	24.262+	25.910	30.017	26.684	29.098	25.068	39.854	31.319	26.622	**22.457**
	WMAPE	33.04%	14.29%	13.94%+	14.88%	17.27%	15.36%	16.73%	14.42%	22.88%	18.04%	15.29%	**12.90%**
60min	RMSE	187.077	113.782	91.921	98.932	90.747	91.453	111.806	88.424	138.327	105.146	79.128+	**74.336**
	MAE	101.024	61.716	50.066	53.705	49.675	51.021	64.656	50.462	84.783	57.853	43.273+	**40.767**
	WMAPE	29.19%	17.75%	14.40%	15.45%	14.29%	14.82%	18.60%	14.52%	24.39%	16.64%	12.45%+	**11.73%**
Average	RMSE	87.068	47.704	43.115	44.655	45.320	43.437	48.862	42.027	57.019	50.395	39.926+	**37.319**
	MAE	46.204	25.978	23.362	24.325	24.728	23.836	27.466	23.339	33.652	27.607	22.391+	**20.522**
	WMAPE	29.33%	16.55%	15.63%	15.89%	16.49%	15.68%	17.13%	15.39	19.45%	18.09%	15.30%+	**14.10%**

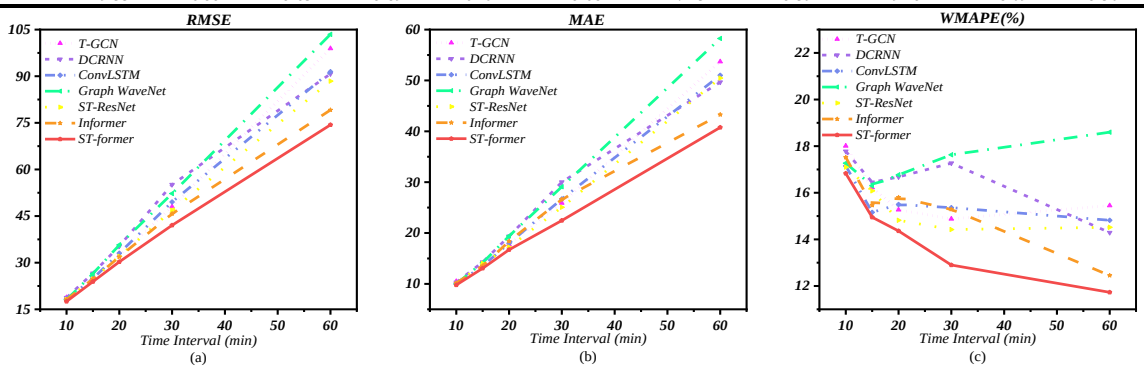

Figure 13 The overall evaluate metrics of methods

Figure13 (c) represents the passenger flow prediction performance of Station C, which is a large transfer hub. Different from the first two stations, Station C does not have obvious commuting characteristics (morning and evening peak characteristics), and its passenger flow is significantly higher than that of the other two stations. There are two peaks of passenger flows in the afternoon and evening, because passengers always arrive in the afternoon. The weekend passenger flow is greater than that on weekdays, which conforms to the general rule that people choose to travel on weekends. Our model utilizes the multi-head self-attention mechanism to model the multi-level temporal dependencies, thus comprehensively describing the changing trend of passenger flow.

In general, ST-former adopts CPSA to capture the local temporal dependencies of passenger flow, utilizes the feature extract block to refine the important features of passenger flow, and leverages the temporal convolution block to learn the global evolution trend of passenger flow, thus achieving the accurate station-level passenger flow prediction. The favorable prediction performances at three different stations verify the robustness of the ST-former, indicating that our model is suitable for different types of station-level passenger flow prediction.

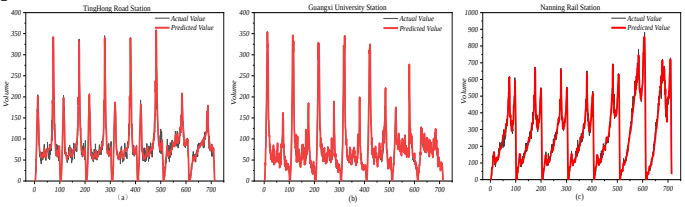

Figure 14 The prediction performance of single station

5.4.3 *Comparison of Rush hours*

To further study the temporal robustness of ST-former, we focus on passenger flow prediction during rush hours. In this section, the rush hours are set to 7:00-9:00 and 17:00-20:00, and the prediction performance of all methods is summarized in Table IV. As can be seen in the Table IV, ST-former still maintains its advantages over other baselines in all cases, which improves the second-best results by 14.22%, 14.14%, and 10.51% in terms of the average RMSE, average MAE, and average WMAPE, respectively. Specifically, ST-former has achieved the optimal prediction performance no matter at which time interval. This is because ST-former can model the changing trends of passenger flow during rush hours, thus accurately predicting the local peaks during rush hours. It is worth noting that Transformer has a particularly poor prediction performance under the 60-time interval while consuming high computation costs. The causal-convolution probsparse self-attention (CPSA) of our model leverages the probsparse self-attention to figure out the problem of high computation cost, and utilize the causal convolution operation to model the local evolution trend of passenger flow during rush hour, resulting in favorable prediction performance of ST-former during rush times. In summary, the extensive experiments on the CityMetro dataset show the effectiveness and robustness of our model during rush hours.

Table IV Performance comparison of different methods on Rush Hours. The best results are emphasized in bold font and the second-best results are labeled with an "+".

Time	Metric	ARIMA	LSTM	CNN	T-GCN	DCRNN	ConvLSTM	GWN	ST-ResNet	Transformer	MGT	Informer	ST-former
10min	RMSE	43.684	26.514	28.222	26.785	25.247	26.440	25.701	25.236+	25.829	28.249	25.820	**23.741**
	MAE	26.214	18.565	18.565	17.871	16.960	16.985	17.013	16.383	16.374+	18.307	16.945	**15.789**
	WMAPE	23.43%	13.90%	14.33%	12.67%	13.10%	13.11%	13.14%	12.65%	12.63%	14.13%	12.36%+	**12.19%**
30min	RMSE	268.521	64.255	66.051	74.908	90.946	71.652	79.395	67.634	98.182	91.484	67.070+	**58.739**
	MAE	88.020	43.492	43.692	49.228	58.586	46.212	51.963	43.261+	67.756	53.834	45.955	**38.646**
	WMAPE	25.92%	11.28%	11.19%	12.67%	15.07%	11.89%	13.37%	11.21%	17.43%	13.85%	10.83%+	**9.94%**
60min	RMSE	355.215	193.988	144.877	150.742	128.138	165.350	179.243	124.037	304.489	168.354	104.107+	**103.586**
	MAE	241.367	134.359	96.206	102.545	82.720	114.538	122.514	85.257	217.989	115.471	**70.573**	70.639+
	WMAPE	29.87%	17.29%	12.38%	13.19%	10.64%	14.74%	15.77%	10.97%	28.05%	15.01%	9.21%+	**9.04%**
Average	RMSE	222.473	94.919	79.717	84.145	81.443	87.814	94.780	72.302+	142.833	96.029	65.666+	**62.022**
	MAE	118.534	65.472	52.754	56.548	52.755	59.245	63.830	48.400+	100.706	62.537	44.824+	**41.558**
	WMAPE	26.41%	14.16%	12.63%	12.84%	12.94%	13.25%	14.09%	11.61%+	19.37%	14.33%	11.30%+	**10.39%**

5.4.4 *Ablation Study*

To further analyze the influences of different components in ST-former, extensive ablation studies are implemented on the CityMetro dataset. The ablation studies are conducted at three different time intervals (10min, 30min, and 60min), and the evaluation metrics are calculated respectively. The results in the following tables are the mean values of the evaluation metrics over all time intervals.

Causal-Convolution ProbSparse Self-Attention: To verify the effectiveness of the Causal-Convolution ProbSparse Self-Attention block, we develop two variants of ST-former:

● ST-former with conventional self-attention: we utilize the conventional multi-head self-attention to replace the probsparse self-attention in the encoder and decoder, aiming to test the advantage of probsparse self-attention. Noting that the causal-convolution operation before calculating the attention scores remains constant.

● ST-former with probsparse self-attention: all causal convolution operations of CPSA are replaced by the linear projection to study the effect of causal convolution for CPSA.

The above models employ the same settings as ST-former except for the self-attention mechanism. The performance metrics of these models are shown in Table VI and Figure 15. As we can see, the results of ST-former with conventional multi-head self-attention are the worst among all cases, because the performance of conventional multi-head self-attention will be limited when calculating the attention scores between all the sequence nodes. As CPSA can exploit the local temporal trend by leveraging the causal convolution, thus endowing ST-former the ability to model the local temporal dependencies. Therefore, ST-former performs better than ST-former with probsparse self-attention. The prediction results fully demonstrate the effectiveness of CPSA in conducting passenger flow prediction.

Table VI Ablation study of the self-attention mechanism

Model	RMSE	MAE	WMAPE
ST-former with Conventional Self-Attention	54.78	30.638	16.08%
ST-former with ProbSparse Self-Attention	46.031	25.132	14.16%
ST-former	**44.639**	**24.337**	**13.82%**

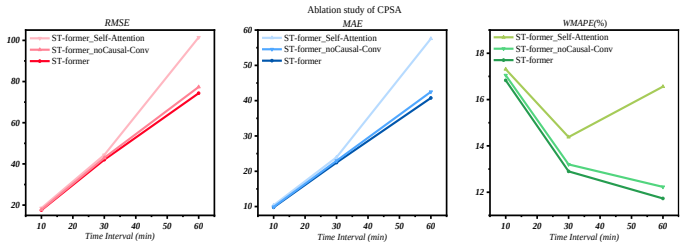

Figure 15 The ablation study of CPSA

Adaptive Multi-Graph Convolution block: To evaluate the effects of the Adaptive multi-graph convolution block, we consider three variants of our model as follows.

● ST-former-single graph: we only consider the adjacent matrix to model the spatial dependencies. The aim is to justify the usage of multiple graphs.

● ST-former with the general graph convolution block: all the adaptive multi-graph convolution blocks are replaced by the conventional GCN blocks to study the advantages of adaptive multi-graph convolution block.

● ST-former without Adaptive multi-graph convolution block: all the Adaptive multi-graph convolution blocks are removed from ST-former to study the contribution of modeling the multi-level spatial dependencies.

The above models employ the same settings as ST-former except for the components studied. The evaluation metrics of these models are reported in Table V and Figure 16. It can be seen that ST-former without AMGCN performs worst among these cases, indicating the importance of considering complex multi-level spatial dependencies of passenger flow In addition, the prediction performance of the ST-former with a single graph is better than that of the ST-former with a general GCN, verifying that the AMGCN is superior to GCN in learning the complex dynamic spatial dependencies. When all available graphs are utilized (adjacent graph, functional similarity graph, OD-based correlation graph), the model achieves the best performance. Such a phenomenon validates the advantages of AMGCN with multiple graphs in dynamic modeling of the complex spatial dependencies of passenger flow.

Table V Ablation study of AMGCN

Model	RMSE	MAE	WMAPE
ST-former with Single Graph	45.823	25.098	14.22%
ST-former with General GCN	46.169	25.126	14.18%
ST-former without AMGCN	46.599	25.376	14.27%
ST-former	**44.639**	**23.337**	**13.82%**

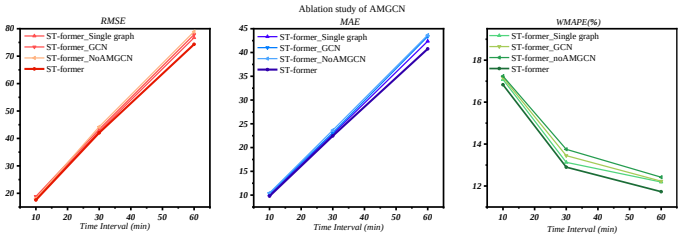

Figure 16 The ablation study of AMGCN

Multi-source data fusion: To study the impact of COVID-19 on passenger flow, all possible combinations of the passenger flow data, the epidemic confirmed data, and the social media data are investigated. It should be noted that all possible data combinations must include passenger flow data because the experiments are focused on the URT passenger flow prediction.

All model parameters are consistent with ST-former except for the input data combinations. Table VII and Figure 17 shows the prediction performance of ST-former with different data combinations. It can be seen that ST-former performs the worst when other relevant epidemic data sources are not considered. When we consider other relevant epidemic data sources, the prediction errors of ST-former have decreased. When we only consider confirmed case data, the performance is worse than that of only considering social media data, because the correlation coefficient between relevant social media data and passenger flow is higher than that between confirmed case data and passenger flow. When ST-former fuses all data sources, it achieves the best prediction performances. The result indicates that fusing the relevant epidemic data sources into the model can help to study the impact of the epidemic on passenger flow and reinforce the temporal features of passenger flow during COVID-19, which can improve the accuracy of epidemic passenger flow prediction.

Table VII Ablation study of data combinations

Data Type			Nanning Metro		
Passenger Flow Data	Confirmed Data	Social Media Data	RMSE	MAE	WMAPE
✔			45.909	25.234	14.54%
✔	✔		45.744	25.107	14.34%
✔		✔	45.631	24.954	14.21%
✔	✔	✔	**44.639**	**24.337**	**13.82%**

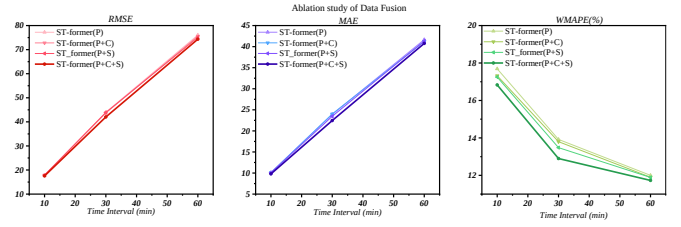

Figure 17 The ablation study of Data Fusion

Feature Extract block: To explain the effectiveness of the feature extract block in our model, we conduct the control variable experiment.

Periodicity Modeling: To further research the influence of periodicity, we develop one variant of ST-former without weekly periodicity and daily periodicity.

The results of the control variable experiment are shown in Table VIII and Figure 18. It is seen that ST-former with single periodicity (only considering the past *TS* time steps historical passenger flow) has the worst evaluation metrics, because there exist certain periodicities in the passenger flow, it usually has a similar evolution trend on weekdays/weekends. The introduction of multiple periodicities is beneficial for ST-former to capture the temporal changing features of passenger flow along multi-dimensions (long-term, medium-term, and short-term) and learn the inherent periodic law of passenger flow, thus improving the prediction accuracy.

The prediction performance of ST-former without the feature extract block is also inferior to ST-former, indicating that the feature extract block can focus on the dominant attention points so as to reinforce the spatiotemporal features of passenger flow. Such experiment results show that the multiple periodicities and feature extract block are irreplaceable for ST-former.

Table VIII Ablation study of Feature Extract Block and Multiple periodicities

Model	RMSE	MAE	WMAPE
ST-former without Feature Extract	46.349	25.558	14.33%
ST-former with Single Periodicity	46.751	26.123	14.60%
ST-former	**44.639**	**24.338**	**13.82%**

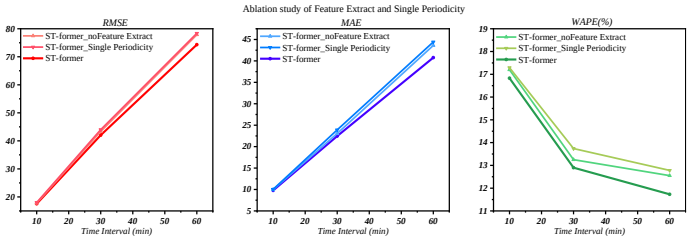

Figure 18 The ablation study of Feature Extract Black and Multiple periodicities

6 CONCLUSION

In this work, we propose a novel deep learning-based model ST-former to conduct the URT passenger flow prediction during COVID-19. It can provide a reliable reference method for passenger flow prediction under public health events. The main contributions are summarized as follows:

- The proposed ST-former has significant advantages to predict the passenger flow during COVID-19, which utilizes the attention mechanism to capture the complex temporal dependencies, and leverages the multi-graphs convolution network to model the dynamic spatial dependencies from different perspectives.
- ST-former fuses the passenger flow data, epidemic-related social media data, and the confirmed cases data to study the impact of COVID-19 and reinforce the changing features of passenger flow, thus enhancing prediction accuracy.

● The results tested in the CityMetro dataset demonstrate the superiority of the ST-former. The improvements compared with the best (existing) method are 5.78%, 8.34%, and 7.84% in terms of RMSE, MAE, and WMAPE, respectively. Extensive ablation studies show the effectiveness and indispensability of some key components in ST-former.

However, there are several limitations to our study. For example, limited by the difficulty of data collection, our model is only tested on the subway dataset, and the effectiveness of ST-former on other traffic modes needs to be further verified. Besides, in addition to the passenger flow prediction during the epidemic, the passenger flow prediction under other unconventional scenarios, such as large-scale sports events, is also of great research significance. In future work, we will expand the data scale to analyze the relationship between passenger flow and COVID-19, thus improving the stability of prediction. We will also attempt to apply this model to the passenger flow prediction under other unconventional conditions, enhancing the generalization of our model.

7 REFERENCES

[1] Cai, P. and Y. Wang (2016). "A spatiotemporal correlative k-nearest neighbor model for short-term traffic multistep forecasting.", *Transportation Research Part C-Emerging Technologies*, Vol. 62, pp. 21-34.

[2] Castro-Neto, M. and Y. Jeong, et al. (2009). "Online-SVR for short-term traffic flow prediction under typical and atypical traffic conditions." *Expert Systems with Applications*, Vol. 3 No. 36, pp. 6164-6173.

[3] Chaniotakis, E. and C. Antoniou (2015). "Use of Geotagged Social Media in Urban Settings: Empirical Evidence on Its Potential from Twitter". *IEEE 18th International Conference on Intelligent Transportation Systems*, pp. 214-219.

[4] Chen, C. and K. Li (2019). "Gated residual recurrent graph neural networks for traffic prediction", *Proceedings of the AAAI conference on artificial intelligence*, Vol. 33 No.01, pp. 485-492.

[5] Chen, E. and Z. Ye (2020). "Subway passenger flow prediction for special events using smart card data." *IEEE Transactions on Intelligent Transportation Systems*, Vol. 3 No. 21, pp. 1109-1120.

[6] Chen, Y. and Y. Lv, et al. (2019). "Detecting Traffic Information from Social Media Texts with Deep Learning Approaches." *IEEE Transactions on Intelligent Transportation Systems*, Vol. 20 No. 8, pp. 3049-3058.

[7] Child, R (2019). "Generating Long Sequences with Sparse Transformer." *arXiv preprints*: arXiv: 1904.10509.

[8] Dwivedi, V. P. and X. Bresson (2020). "A generalization of Transformer Networks to Graphs." *arXiv preprint*: arXiv: 2012.09699.

[9] Guo, J. and W. Huang (2014). "Adaptive Kalman filter approach for stochastic short-term traffic flow rate prediction and uncertainty quantification." *Transportation Research Part C: Emerging Technologies*, Vol. 43, pp. 50-64.

[10] Guo, K. and Y. Hu (2021). "Optimized graph convolution recurrent neural network for traffic prediction." *IEEE Transactions on intelligent transportation systems*, Vol. 22 No. 2, pp. 1138-1149.

[11] He, J. and W. Shen (2013). "Improving traffic prediction with Tweet semantics". *Twenty-Third International Joint Conference on Artificial Intelligence*. pp.1387-1393.

[12] Jiao, F. and L. Huang (2021). "An Improved STL-LSTM Model for Daily Bus Passenger Flow Prediction during the COVIN-19 Pandemic." Sensors Vol. 17 No. 21, pp. 5950.

[13] Kipf, T. N. and M. Welling (2016). "Semi-supervised classification with Graph Convolutional Networks.", *International Conference on Learning Representations* (ICLR).

[14] Kumar, S. V. and L. Vanajakshi (2015). "Short-term traffic flow prediction using seasonal ARIMA model with limited input data." European Transport Research Review. Vol 7 No. 3, pp.1-9.

[15] Lea, C. and M. D. Flynn (2017). "Temporal Convolutional Networks for Action Segmentation and Detection". *Proceedings of the IEEE Conference on Computer Vision and Pattern Recognition*. pp. 156-165.

[16] Li, S. and X. Jin, et al. (2019). "Enhancing the Locality and Breaking the Memory Bottleneck of Transformer on Time Series Forecasting." Advances in Neural Information Processing Systems. Vol. 32, pp. 1-11.

[17] Li, Y. and R. Yu (2018). "Diffusion convolutional recurrent neural network: data-driven traffic forecasting." *International Conference on Learning Representations* (ICLR).

[18] Lippi, M. and M. Bertini (2013). "Short-Term Traffic Flow Forecasting: An Experimental Comparison of Time-Series Analysis and Supervised Learning." *IEEE Transactions on Intelligent Transportation Systems*. Vol. 2 No. 14, pp. 871-882.

[19] Liu, X. and X. Kong (2016). "Collective traffic prediction with partially observed traffic history using location-based social media." *Proceedings of the 25th ACM International on Conference on Information and Knowledge Management*. pp. 2179-2184.

[20] Lv, Z. and J. Li (2021). "Deep learning in the COVID-19 epidemic: A deep model for urban traffic revitalization index." *Data & Knowledge Engineering*. Vol. 2021 No. 135, pp. 101912.

[21] Ma, X. and Z. Dai (2017). "Learning traffic as image: A deep convolutional neural network for long-scale transportation network speed prediction." *Sensors*. Vol. 4 No. 17, pp. 818.

[22] Ma, X. and Z. Tao, et al. (2015). "Long short-term memory neural network for traffic speed prediction using remote microwave sensor data." Transportation Research Part C: Emerging Technologies. Vol. 54, pp. 187-197.

[23] Ni, M. and Q. He, et al. (2014). "Using Social Media to Predict Traffic Flow under Special Event Conditions." *The 93rd annual meeting of Transportation Research Board*. pp.1-23.

[24] Ni, M. and Q. He, et al. (2017). "Forecasting the Subway Passenger Flow Under Event Occurrences with Social Media." *IEEE Transactions on Intelligent Transportation Systems*. Vol. 18 No. 6, pp 1623-1632.

[25] Roy, K. C. and S. Hasan, et al. (2021). "Predicting traffic demand during hurricane evacuation using Real-time data from transportation systems and social media." *Transportation Research Part C: Emerging Technologies*. Vol 131 No. 2021, pp. 103339.

[26] Sun, Y. and B. Leng (2015). "A novel wavelet-SVM short-time passenger flow prediction in Beijing subway system." *Neurocomputing*. Vol. 2015 No. 166, pp. 109-121.

[27] Vaswani, A. and N. Shazeer, et al. (2017). "Attention Is All You Need." *Advances in neural information processing systems*. Vol. 30, pp. 1-15.

[28] Voort, M. V. D. and M. Dougherty (1996). "Combining Kohonen maps with ARIMA time series Models to forecast traffic flow."

Transportation Research Part C: Emerging Technologies. Vol. 5 No. 4, pp. 307-318.
[29] Woo, S. and J. Park (2018). "Convolutional Block Attention Module ". *Proceedings of the European conference on computer vision* (ECCV). pp.3-19.
[30] Wu, Z. and S. Pan (2019). "Graph WaveNet for deep spatial-temporal graph modeling." *Proceedings of the 28th International Joint Conference on Artificial Intelligence*. pp. 1907-1913.
[31] Xingjian, S. and Z. Chen, et al. (2015). "Convolutional LSTM network: A machine learning approach for precipitation nowcasting." *Advances in Neural Information Processing Systems*. Vol. 28, pp. 1-9.
[32] Xue, G. and S. Liu, et al. (2022). "Forecasting the subway passenger flow under event occurrences with multivariate disturbances." *Expert Systems with Applications*. Vol. 188, pp. 116057.
[33] Yan, H. and X. Ma (2021). "Learning Dynamic and Hierarchical Traffic Spatiotemporal Features with Transformer." *IEEE Transactions on Knowledge and Data Engineering*. pp. 1-14.
[34] Yang, H. and T. S. Dillon (2018). "Optimized configuration of exponential smoothing and extreme learning machine for traffic flow forecasting." *IEEE Transactions on Industrial informatics* Vol. 15 No. 2018, pp. 23-34.
[35] Yang, H. and X. Li (2021). "A network traffic forecasting method based on SA optimized ARIMA-BP neural network." *Computer Networks* Vol. 193 No.2021, pp. 108102.
[36] Yao, H. and X. Tang (2019). "Revisiting spatial-temporal similarity: A deep learning framework for traffic prediction. " *Proceedings of the AAAI conference on artificial intelligence*.
[37] Yao, W. and S. Qian (2021). "From Twitter to traffic predictor Next-day morning traffic prediction using social media data." *Transportation Research Part C-Emerging Technologies*. Vol. 124 No. 2021, pp. 102938.
[38] Ye, X. and S. Fang (2022). "Meta Graph Transformer A Novel Framework for Spatial-Temporal Traffic Prediction." Neurocomputing. Vol. 491 No. 2022, pp. 544-563.
[39] Yu, B. and H. Yin (2017). "Spatio-Temporal Graph Convolutional Networks: A deep learning framework for traffic forecasting." *Proceedings of the 27th International Joint Conference on Artificial Intelligence*. pp. 3636-3640.
[40] Yu, B. and Y. Lee (2020). "Forecasting road traffic speeds by considering area-wide spatiotemporal dependencies based on a graph convolutional neural network (GCN)." *Transportation Research Part C-Emerging Technologies*. Vol. 114, pp. 189-204.
[41] Zhang, J. and F. Chen (2020). "Multi-Graph Convolutional Network for Short-Term Passenger Flow Forecasting in Urban Rail Transit." *IET Intelligent Transport Systems* Vol. 14, pp. 1210-1217.
[42] Zhang, J. and Y. Zheng, et al. (2017). "Deep Spatio-Temporal Residual Networks for Citywide Crowd Flows Prediction". *Thirty-first AAAI conference on artificial intelligence*.
[43] Zhang, W. and C. Zhang (2021). "Transformer Based Spatial-Temporal Fusion Network for Metro Passenger Flow Forecasting". *IEEE 17th International Conference on Automation Science and Engineering* (CASE), Lyon, France.
[44] Zhao, L. and Y. Song, et al. (2020). "T-GCN: a temporal graph convolutional network for traffic prediction." *IEEE Transactions on Intelligent Transportation Systems* Vol. 21 No. 9, pp. 3848-3858.
[45] Zhou, H. and S. Zhang, et al. (2020). "Informer: Beyond Efficient Transformer for Long Sequence Time-Series Forecasting." Proceedings of the AAAI Conference on Artificial Intelligence. Vol. 35 No. 12, pp. 11106-1115.

Shuxin Zhang was born in Guangdong Province, China. He is a master in Beijing Jiaotong University. His research interests include machine learning, deep learning, traffic data mining and applications, and dynamic traffic modeling and management.

Jinlei Zhang was born in Hebei Province, China. He received a Ph.D. degree from Beijing Jiaotong University, China. He is currently an assistant professor at Beijing Jiaotong University. His research interests include machine learning, deep learning, traffic data mining and applications, and dynamic traffic modeling and management.

Lixing Yang received the B.S. and M.S. degrees from the Department of Mathematics, Hebei University, Baoding, China, in 1999 and 2002, respectively, and the Ph.D. degree from the Department of Mathematical Sciences, Tsinghua University, Beijing, China, in 2005.

Since 2005, he has been with the State Key Laboratory of Rail Traffic Control and Safety, Beijing Jiaotong University, Beijing, where he is currently a Professor. He is the author or co-author of more than 80 papers published in national conferences, international conferences, and premier journals. His current research interests include stochastic programming, fuzzy programming, intelligent systems, and applications in transportation problems and rail traffic control systems.

Chengcheng Wang received the B.S. and Ph.D. degrees in Central South University, Changsha , China, in 2015,and 2020, respectively. She is currently working as an engineer in Shandong Provincial Communications Planning and Design Institute Group Co. LTD. Her research interests include traffic data mining, complex network, traffic modeling and management.

.

Ziyou Gao received the Ph.D. degree from the Institute of Applied Mathematics, Chinese Academy of Sciences, Beijing, China, in 1994. He is currently a Professor with the State Key Laboratory of Rail Traffic Control and Safety, Beijing Jiaotong University. He also serves as the President of the Society of Management Science and Engineering of China, the Vice-President of the Systems Engineering Society of China, and the Vice-President of the Chinese Society of Optimization, Overall Planning and Economic Mathematics. In 2003, he was elected as a foreign member of the Russian Academy of Natural Sciences. His research interests include management and optimization of urban rail transit, complexity of transportation network, and transport modeling and planning.